[illegible] Washington [illegible] October [illegible], 1991

Electrical Impedance Imaging in Two-Phase, Gas-Liquid Flows: 1. Initial Investigation

J.T. Lin[1], L. Ovacik[2], O.C. Jones[3]
Center for Multiphase Research, Rensselaer Polytechnic Institute
Troy, New York 12180-3590 U.S.A.

ABSTRACT

The determination of interfacial area density in two-phase, gas-liquid flows is one of the major elements impeding significant development of predictive tools based on the two-fluid model. Currently, these models require coupling of liquid and vapor at interfaces using constitutive equations which do not exist in any but the most rudimentary form. Work described herein represents the first step towards the development of electrical impedance computed tomography (EICT) for nonintrusive determination of interfacial structure and evolution in such flows.

INTRODUCTION

Description of interfacial structure and evolution, as well as the gradients which control transfer of mass, momentum, and energy at these phase boundaries is the single most important key element and the challenge for the future of two-phase flow analysis. Indeed, measurement and prediction of phase boundary structure and gradients at these boundaries is one of the major factors impeding development of true predictive capability for systems involving flows of liquid and vapor or gas mixtures.

There are no methods available today which allow determination of interfacial structure and evolution in any but the most simplistic cases. It is the purpose of this paper to describe a concept which appears to hold promise for determining the distribution and evolution of interfacial area density in two-phase, gas-liquid flows.

BACKGROUND

The concept of impedance imaging includes a body of unknown internal electrical field properties of conductivity and permittivity surrounded by electrodes on the bounding surface. These electrodes are excited electrically either in pairs or groups, and the response on the entire set of electrodes is determined. The excitation can be either applied current (AC) or applied voltage (AV), and the measured response can be similar. This is undertaken for all linearly independent combinations of excitation and response to provide numerous sets of data which can then be used to form an image. Maxwell's equations for the behavior of the electrical field are utilized to determine the internal distribution of electrical properties which minimizes (in the least squares sense) the difference between the computed boundary response (given the excitation) and the measured response. If there are N-electrodes, and all possible independent combinations of excitation and response are utilized, there are N(N-1)/2 independent measurements which allows the field to be broken into the same number of regions within which the conductivity and/or permittivity can be determined. The challenge is to develop an accurate and rapid tomography system coupled with accurate inverse computational methods which will allow clear images to be determined.

---

1. Post-Doctoral Research Associate
2. Graduate student
3. Professor of Nuclear Engineering and Engine
and Director--Center for Multiphase Research

Research in the development of electrical impedance computed tomography (EICT) has been undertaken in the geological area [c.f. Dynes and Lytle[1]] and in the biomedical field [c.f. Seagar, Barber, and Brown[2]]. Most methods have used the resistive field because the resistivities of relevant materials are low. To date, the best of applications applied to real systems produce a very fuzzy planar "picture" of resistivity or permittivity variations but the results are encouraging.

Most EICT methods can be classified by the number of poles used to make a single measurement, and the method of excitation. Two-pole methods use only two electrodes for both excitation and measurement whereas four-pole methods separate excitation electrodes from those used for measurement, the measurement generally being a potential difference. Some feel that the four-pole method eliminates errors due to contact resistance at excitation electrodes, but this is not clearly a benefit [Newell et al.[3,4]].

Price[5], although unsuccessful, appears to have been the first in the biomedical field to attempt obtaining impedance tomographs using the three-pole method but his reported work failed. His suggestion of the use of "guarding" methods was followed by others, all of whom were unsuccessful [Bates et al.[6], Schneider[7], Seagar et al.[2]]. Furthermore, in the three-pole method, small voltage differences are obtained by subtracting the measured voltages leading to substantial errors [Smith[8]].

Contact impedance was minimized by Barber et al.[9], using a two-pole method and high-impedance measurement methods, but results were quite blurred. Two-pole methods were also used with little success by Dynes and Lytle[1] and by Starzyk and Dai[10].

Seagar et al.[11] contend that the blurring of two-dimensional results in a continuously variable conservative field is due to nonzero effective wave number (infinite wave length) of the applied signal. They show, however, that successful reconstructions can be made for certain classes of piecewise constant media (similar to two-phase systems), and that the process is relatively simple when the discrete zones are circular in shape.

There can be orders of magnitude differences between the sensitivity of a given boundary measurement to a fixed size body depending on its location. Similar orders difference can thus occur in the eigenvalues of the solution matrix thereby making the inversion problem severely ill-posed and difficult to solve [Tarassenko and Rolph[12], Murai and Kagawa[13,14]]. In spite of ill conditioning, good results were obtained by Wexler[15] using a four-pole potential method with real domain reconstructions even where there were widely varying conductivities in an overall conducting medium--i.e., metal and plastic shapes in a conducting water field.

Isaacson and coworkers [Isaacson[16], Gisser, Isaacson, and Newell[17], Isaacson and Cheney[18]] described a method to estimate the conditions necessary to distinguish a homogeneous cylindrical body of one size, centered in a cylinder of a larger size with the region between the two also of homogeneous electrical field structure. This was followed by Fuks et al.[34] who also provided methods of estimating the degree of accuracy to be obtained with digital conversion of data. In general, they found that increasing the number of electrodes can improve the image only up to a point after which better imaging comes only by improving accuracy of measurement.

Barber and Brown[19,20] developed an iterative back-projection method based on linearization around a constant conductivity. This method was subsequently improved upon by Santosa and Vogelius[21] but with mixed results. Beck and his co-workers [Huang, et al.[22], Beck and Williams[23]] have also developed back-plane projection methods for analysis of gas-liquid pipe flows of gas and oil. A variational method developed by Kohn and Vogelius[24] is similar to that of Wexler et al.[15] but guaranteed to converge. It was shown by Kohn and McKenney,[25] however, to produce results no better than those of Wexler[15]. Murai and Kaga-

wa[13] used a "matrix regularization" method based on Akaike's information criterion and eliminated altogether the problem of ill-conditioning.

Yorkey, Webster, and Tompkins (YWT) followed a different approach using Marquardt's conditioning method which they stated to be better than Akaike's method. Their results appear singularly successful in inversion of two carefully-chosen numerical experiments [Yorkey[26], Yorkey and Webster[27], Yorkey, Webster, and Tompkins,[28-31]]. Finite element methods were used to obtain accurate reconstructions in four iterations. No reconstruction of real situations has yet been reported and Kohn and McKenney[25] indicate the YWT tests were "biased by the nature of the synthetic data."

Very slow transient results were obtained by Brown, Barber, and Seagar[32] when a dish of heated saline solution was reconstructed showing the thermal patterns of convection. From comparison of their results with Price's estimates of resistivity [Price[5]] it seems that changes of the order of 1.5-10 Ω-cm were easily resolved. These results also indicate that there is a good potential for application of EICT methods to natural convection studies.

Finite element methods seem to have been singularly useful in reconstruction tomography of electrical fields. Starting with the suggestions of Kim, Tompkins, and Webster[33], this work has been the basis for the most successful inversions reported on to date [Dynes and Lytle[1], Murai and Kagawa[13], and Yorkey[26-31]].

Yorkey et al.[31] examined several other methods including the perturbation method used by Kim et al.[33], the equipotential lines method used by Barber et al.[9] and by Barber and Brown[20], the iterative equipotential lines method (the original one proposed did not iterate), and the method used by Wexler et al., and similarly by Kohn and Vogelius[24] (referenced by YWT). Of the five methods tried, only the YWT method converged to zero error in overall resistivity, and seemed to obtain the correct result locally, in spite of the fact that they only utilized adjacent electrodes for excitation--a pattern guaranteed to produce the most difficult problems with sensitivity. Other methods either did not converge or converged with some error.

On a completely separate track, Newell, Gisser, and Isaacson and their coworkers at Rensselaer have been developing the multi-pole current distribution (MPCD) method. This method has resulted from mathematical analysis showing the "best" application of electrical current in a radially-symmetric system to be $\sin(k\theta)$ and $\cos(k\theta)$, $k=1...K$ where K is half the number of circumferential electrodes [Gisser et al.[17], Newell et al.[3,4], Fuks et al.[34], Isaacson and Cheney[18], Cheng et al.[35]]. This distribution is optimum in effect because at any instant all electrodes are simultaneously excited and the total input current is the sum of individual electrode-pair currents thereby increasing the sensitivity and decreasing the effects of noise in the system. Results on two-dimensional electrode arrays without iteration (Newton One Step Error Reconstruction, NOSER, method[36]) are quite fuzzy but are the equal of others described in the literature.

ANALYSIS

Reconstruction Method

The iterative method showing most rapid convergence (Yorkey's resistive network or YWT method) was extended to complex reactive networks. The computational logical includes two parts. The first part is the forward problem which is used to generate a voltage distribution using a given distribution of complex conductivity. The second part is the inverse problem which uses the calculated boundary voltages in comparison with the measured values to reconstruct the conductivity/ permittivity distribution.The theoretical basis for the algorithm is given as follows. The steady-state governing equation for the voltage distribution within the inhomogeneous and isotropic field is given by the equation

$$\nabla \cdot (\sigma \nabla V) = 0. \tag{1}$$

where V is the voltage field and $\sigma = (c + j\omega\varepsilon)$, c being the conductivity, ε the permittivity, and ω the frequency. Finite element methods (FEM) are utilized where they are nodalized by quadrilateral elements then transformed to squares for computational purposes. It is known that this method converges to the exact solution where the element size becomes infinitesimal.

The FEM is defined for a reactive network as YV = C, such that the voltage field is given as

$$\mathbf{V}_{NxP} = \mathbf{Y}^{-1}_{NxN}\mathbf{C}_{NxP}. \tag{2}$$

where **Y** is the N x N indefinite admittance-matrix. The matrix-size parameters are defined as

N	= the number of nodes
P	= the number of current excitations
M	= the number of elements
E	= the number of external measurement electrodes

While **V** represents the voltages of the nodes both inside and on the periphery of the body, a transformation is made to extract the calculated boundary voltages from the calculated voltage matrix $\mathbf{V}_{NxP}$ to form a new vector $\mathbf{f}_{EPx1}$. The measured voltages on the E-electrodes with P-current excitations are collected to form the vector $\mathbf{V}_{0,EPx1}$.

There are differences between the calculated voltages $\mathbf{f}_{EPx1}$ and measured voltages $\mathbf{V}_{0,EPx1}$ on the electrodes. A scalar error function is defined as

$$\phi = \frac{1}{2}[\mathbf{f} - \mathbf{V}_0]^T[\mathbf{f} - \mathbf{V}_0]. \tag{3}$$

In order to get minimum error, the differential of ϕ relative to σ should vanish. Thus,

$$\phi' \equiv \frac{d\phi}{d\sigma} = [\mathbf{f}']^T[\mathbf{f} - \mathbf{V}_0] = 0 \tag{4}$$

where $\mathbf{f}' = d\mathbf{f}/d\sigma$. The quantity ϕ' can be expressed as a Taylor expansion

$$\phi' \cong \phi'(\sigma^K) + \phi''(\sigma^K)\nabla(\sigma^K) = 0. \tag{5}$$

Thus, since ϕ' vanishes, the gradient of the conductivity is given by

$$\nabla\sigma^K = -[\phi''(\sigma^K)]^{-1}\phi'(\sigma^K) \tag{6}$$

where

$$\phi' = [\mathbf{f}'(\sigma^K)]^T[\mathbf{f}(\sigma^K) - \mathbf{V}_0] \tag{7}$$

and where

$$\phi''(\sigma^K) \cong [\mathbf{f}'(\sigma^K)]^T\mathbf{f}'(\sigma^K). \tag{8}$$

The corrections to σ^K can be obtained after every iteration, until the convergence criteria is met.

A areasonable level of spatial resolution will need many current excitations and so the matrices required in the inversions can be very large. Since the forward computation of the field potential for a given complex resistivity pattern involves inversion of a sparse matrix, Gaussian elimination methods used are computationally expensive. Thus, the Jacobi conjugate gradient (JCG) method (similar to that described by Carey and Oden[45]) has been utilized for real domain inversions. Time savings was achieved by maintaining a constant Jacobian for several iterations.

In the case of a matrix having eigenvalues separated by orders of magnitude, preconditioning is obtained by pre-multiplying with the inverse of the diagonal or tridiagonal of the original matrix. The JCG

method is both extremely fast and absolutely convergent for positive definite matrices such as are anticipated in this problem. Since it is not necessary to calculate and store zeros in the matrix, the computational CPU time is decreased substantially.

The accuracy for both methods are similar. Hestenes and Stiefel[46] have shown that if the conjugate directions are chosen as the unit basis vectors, then the conjugate gradient will be equivalent to Gaussian Elimination method. Round-off error can also be corrected in the JCG algorithm.

Quadrilateral Mesh Scheme

All computations were undertaken in a dimensionless array of square elements. To easily model geometries having curved surfaces, a transformation from quadrilateral to square elements was included both for preprocessing and postprocessing of computed results.

The sketch in Fig. 1 shows the quadrilateral transformation scheme. Transformation was accomplished in the standard fashion. A shape function $N_i = N_i(\xi,\eta)$ is chosen with the values of ξ and η defined in the figure such that the mapping from the parent domain **R** into the square-element domain. An infinitely small area is transformed using the Jacobian with the following shape functions

$$\begin{aligned} N_1 &= (1/4)(1-\xi)(1-\eta) \\ N_2 &= (1/4)(1+\xi)(1-\eta) \\ N_3 &= (1/4)(1+\xi)(1+\eta) \\ N_4 &= (1/4)(1-\xi)(1+\eta) \end{aligned} \tag{9}$$

A bilinear expansion form is utilized such that

$$\begin{aligned} x(\xi,\eta) &= \alpha_0 + \alpha_1\xi + \alpha_2\eta + \alpha_3\xi\eta \\ y(\xi,\eta) &= \beta_0 + \beta_1\xi + \beta_2\eta + \beta_3\xi\eta \end{aligned} \tag{10}$$

where the α's and β's are determined by the transformation Jacobian

$$\mathrm{J} = \begin{bmatrix} \alpha_1 + \alpha_3\eta & \alpha_2 + \alpha_3\xi \\ \beta_1 + \beta_3\eta & \beta_2 + \beta_3\xi \end{bmatrix}. \tag{11}$$

Now the problem to be solved is Eq. (1). It is assumed that the conductivity is piecewise continuous being constant in each element such that Laplace's equation is solved element-by-element. Thus

$$V = \sum_{i=1}^{4} V_i N_i \quad \text{and} \quad \nabla V = \sum_{i=1}^{4} V_i \ \nabla N_i. \tag{12}$$

Solving Eq. (1) is equivalent to minimizing the functional

$$F = \frac{\sigma}{2} \int\int_{\mathbf{R}} |\nabla V|^2 dS \tag{13}$$

where **R** designates the region occupied by the individual elements for which Eq. (13) applies. Thus,

$$\frac{\partial F}{\partial V_i} = 0 \qquad \text{for} \qquad i = 1,4 \tag{14}$$

which, after minimizing, results identically in Eq. (2). The admittance elements are given by the transformation,

$$Y_{ij} = \sigma_R \int_{-1}^{1}\int_{-1}^{1} F_{ij}\ (\xi,\eta) d\xi d\eta \tag{15}$$

and where

$$F_{ij}(\xi,\eta) = \left(J_{11}^{-1}\frac{\partial N_i}{\partial \xi} + J_{12}^{-1}\frac{\partial N_i}{\partial \eta}\right)\left(J_{11}^{-1}\frac{\partial N_j}{\partial \xi} + J_{12}^{-1}\frac{\partial N_j}{\partial \eta}\right) + \left(J_{21}^{-1}\frac{\partial N_i}{\partial \xi} + J_{22}^{-1}\frac{\partial N_i}{\partial \eta}\right)\left(J_{21}^{-1}\frac{\partial N_j}{\partial \xi} + J_{22}^{-1}\frac{\partial N_j}{\partial \eta}\right) \quad (16)$$

RESULTS

Numerical

Square-element conductive arrays. Duplication of Yorkey's results required implementation of the method using square elements in the resistive mode only. Results obtained were identical to those found by Yorkey et al. Convergence is very rapid with the error function [Eq. (3)] for an 8 x 8 array converging to two significant figures within 4–5 iterations and within 1 part in 10^4 within 12 iterations where the contrast ratio is as large as 10,000:1. Aitken's method is also used to improve convergence speed more than a factor of 3.

Quadrilateral-element arrays. Both real and complex conductivity calculations have been undertaken; however, the real patterns converge much more readily than the complex. Varying Marquardt's constant and not recalculating the Jacobian matrix every iteration leads to nonuniform convergence.

Figure 2 shows two patterns with the number of iterations required for convergence with the fill pattern key between the two reconstructions. The original pattern is chosen to be uniform of high conductivity. Gauss elimination was used to perform matrix inversions. The ring pattern converges much more rapidly than the annular pattern because the zones requiring the greatest changes are nearer the boundary. Furthermore, the central region required no change whereas for the annular geometry, the central zones required maximum change.

Figure 3 shows the convergence sequence for a 64-element body with real-conductivity elements of 3:1 contrast ratio distributed in a relatively arbitrary pattern. The quantitative resistivity pattern definition is identical to that shown at the center of Fig. 2. It is seen that there is a relatively rapid convergence for elements near the boundary even though the change is from one extreme to the other. On the other hand, changes in the central region require significantly more computations for convergence due to the extreme lack of sensitivity of regions farthest from the boundaries. Global error for the three cases (arbitrary, ring, and annular) is shown in Fig. 4, confirming that the more complex the pattern, the larger the number of iterations required for convergence.

The question of noise and error generally pose real difficulties in the convergence of an inverse problem to its solution. In the case of the annular geometry, Gaussian noise was added to the "measured" voltages and the problems recomputed. As shown in Fig. 5, the global error generally decreases until the effects of the error become important and then become relatively constant. Figure 6 shows the variation in the local error for each of the four ring layers in the geometry showing increasing error with distance from the boundary. In the case of 1% Gaussian noise, the local error in the inner elements is above 30%. Even in this case, however, the noise has little effect on the visual recognition of the pattern (Fig 7).

Computation for these 8x8 reconstructions required approximately 3 minutes on the IBM 3090 computer. Of interest was the computational time required for a significantly larger problem, in addition to the interest in gaining better computational resolution. For this purpose, a 256-element pattern (16x16) was computed in two steps: starting with a uniform background pattern using an 8x8 mesh; switching to a 16x16 pattern when convergence ceased due to the effective noise in the system caused by nonalignment of pattern and mesh. Starting with an 8x8 pattern, and using a conjugate gradient method for matrix inversion, convergence is rapid at first, then slows as the effective noise becomes dominant. Switching to a grid

Third International Conference on Inverse Design Concepts and Optimization in Engineering Sciences (ICIDES-III) Editor: G.S. Dulikravich, Washington D.C. October 23-25, 1991

size of 16 x 16 results again in rapid convergence. Computation time in this case for a total of 30 iterations was 43 minutes on the IBM 3090 and convergence was not achieved, even though the global error was reduced to 0.00086. A 24 x 24-element problem required 54 minutes for a single iteration.

EXPERIMENTAL

An example of a electrical impedance tomographic image obtained using sinusoidal current excitation patterns at 15 kHz, and complex conductivity inversion is shown in Fig. 8 (NOSER method, Newell et al.[36]). The test geometry used is a rather shallow, two-dimensional bath 500-mm in diameter. Water filled the dish to a depth of approximately 12 mm except for an empty, 50-mm- diameter beaker placed in the center of the dish.

The NOSER method is a noniterative reconstruction which uses exact solution of the uniform field problem and exact computation of the first Taylor-series corrections in the iterative process. The results shown in Fig. 8 indicate the darker regions where higher impedances associated with air are calculated. In this case, the contrast associated with the central region is only approximate as, for air at 15 kHz excitation the impedance is virtually infinite in comparison with tap water where the resistivity is in the range of hundreds of ohm-cm. The results show that it is clearly possible to separately identify large separate regions of gas-phase surrounded by water in a large geometry, even without iteration.

CONCLUSIONS

A potentially useful method for electrical impedance imaging of two-phase fluid distributions methods has been discussed. The method solves the inverse problem where the internal conductivity field is piecewise approximated using iterative procedures which require computed boundary measurements converge to measured values which exist due to given boundary excitation. Convergence is undertaken in a manner which minimizes the least squares error between the computations and the measurements. Specific results of this work are:

1. The internal distribution of complex electrical impedance can be piecewise approximated within a body by using only boundary excitation and measurement.

2. Square-element FEM modeling of a resistive body allows iterative convergence to 1% within 4-5 iterations and within 0.01% within 12 iterations for all contrast ratios up to 10^5.

3. Quadrilateral-element, FEM modeling was slower to iterate and more sensitive to contrast ratio, perhaps due to the presence of highly acute or obtuse angles distorting the equivalent square-element conductivity. Local error in a given element was shown to be considerably slower to converge to a reasonable error. Elements farthest from the boundary showed slowest convergence, and more complex situations appear to require more iterations for convergence.

4. Complex contrast ratios as large as 10^2 were found to converge using Gauss elimination for matrix inversion. Situations with larger contrast diverged.

5. The computational methods utilized appear quite tolerant to Gaussian noise allowing inverse computations to be undertaken with as much as 1% rms noise in boundary "measurements." The global error is found to diverge from the no-noise case and arrive at a relatively constant value dependent on the noise. Even with relatively large local errors, visual discrimination of the patterns was easily possible.

6. Application to a practical, laboratory situation shows that even without iteration, reasonable results can be obtained for complex conductivity fluids.

ACKNOWLEDGEMENTS

This research was supported by the Energy Research Laboratory, Hitachi, Ltd., Hitachi-shi, Ibaraki-ken, Japan, and by the U.S. Department of Energy under contract number DE-FG07-90ER13032.

NOMENCLATURE

English

c	Conductivity
C	Current matrix
f	Calculated boundary voltage vector
J	Jacobian
N	Shape function for quadrilateral transformation
V	Voltage field
V	Voltage matrix
x	Cartesian coordinates
y	Cartesian coordinate
Y	Admittance matrix

Greek

α	Expansion coefficient
β	Expansion coefficient
ε	Permittivity
ϕ	Scalar error function
η	Transformed coordinate
ω	Radial frequency
σ	Complex conductivity ($c + j\omega\varepsilon$)
ξ	Transformed coordinate

Subscripts and Superscripts and Others

E	Number of measurement electrodes on boundary
i	Matrix element index
j	Matrix element index
K	Iteration number
M	Total number of elements
N	Total number of nodes
P	Number of current excitations
0	Measured

REFERENCES

1. Dynes, K.A., and Lytle, R.J., [1981] "Analysis of electrical conductivity imaging," **Geophysics, 46**, pg. 1025-1036.

2. Seagar, A.D., Barber, D.C., and Brown, B.H., [1987] "Electrical Impedance Imaging," **IEE Proc. 134, Pt. A**, No. 2, pg. 201-210.

3. Newell, J.C., Isaacson, D., and Gisser, D.G. [1989] "Rapid Assessment of Electrode Characteristics for Impedance Imaging," **IEEE-Trans., Biomed. Eng.**, in press.

4. Newell, J.C., Gisser, D.G., and Isaacson, D., [1988] "An Electric Current Tomograph," **IEEE-Trans. Biomed. Eng., 35** (10), pg. 828-833.

5. Price, L.R., [1979] "Electrical impedance computed tomography (ICT): a new CT imaging technique," **IEEE Trans. Nucl. Sci. (USA), NS-26, 2**, pg. 2736-2739.

6. Bates, R.H.T., Mckinnon, G.C., and Seager, A.D., [1980] "A limitation on systems for imaging electrical conductivity distributions," **IEEE Trans. Biomed. Eng., BME-27, 7**, pg. 418-420.

7. Shomberg, H., and Tasto, M., [1981] "Reconstruction of spatial resistivity distribution," Phillips GMDH, Hamburg, Germany (FRG), MS-H 2715/81.

8. Smith, D.N., [1985] "Determination of impedance using numerous simultaneous currents (DINSC) - system design and practical applications," **IEEE Conf. Publ. (Inst. Electr. Eng.)**, No. 257, pg. 69-73

9. Barber, D.C., Brown, B.H., and Freeston, I.L., [1983] "Imaging spatial distributions of resistivity using applied potential tomography," **Elec. Lett., 19**, pg. 933-935.

10. Starzyk, J.A., and Dai, H., [1985] "Element evaluation in the resistive networks," **Midwest Sym. Circuits Syst., 28**, pg. 178-181

11. Seagar, A.D., Yeo, T.S., and Bates, R.H.T.,[1984] "Full wave computed tomography, part 2: Resolution limits," **Proc. IEE, part A, 131**, pg. 616-622.

12. Tarassenko, L., and Rolfe, P., [1984] "Imaging spatial distributions of resistivity - an alternative approach," **Electron. Lett., 20,** 14, pg. 574-576.

13. Murai, T., and Kagawa, Y., [1985] "Electrical impedance computed tomography based on a finite element model," **IEEE Trans. Biomed. Eng.,**

BME-32, 3, pg. 177-184.

14. Murai, T., and Kagawa, Y., [1986] "Boundary element iterative techniques for determining the interface boundary between two Laplace domains-a basic study of impedance plethysmography as an inverse problem," **Int. J. Numer. Methods Eng. (GB), 23**, 1, pg. 35-47

15. Wexler, A., Fry, B., and Neiman, M.R., [1985] "Impedance-computed tomography algorithm and system," **Appl. Opt., 24**, 23, pg. 3985-3992.

16. Isaacson, D., [1986] "Distinguishability of Conductivities by Electric Current Computed Tomography," **IEEE Med. Imaging MI-5**, 91-95.

17. Gisser, D.G., Isaacson, D., and Newell, J.C., [1987] "Current Topics in Impedance Imaging," **Clin. Phys. Physiol. Meas., 8**, Suppl. A, pg. 39-46.

18. Isaacson, D., and Cheney, M., [1990] "Current Problems in Impedance Imaging," in **Inverse Problems in Partial Differential Equations**, D. Colton, R. Ewing, and W. Rundell, Eds., SIAM, Philadelphia.

19. Barber, D.C., and Brown, B.H., [1984] "Applied Potential Tomography," **J. Phys. E: Sci. Instrum., 17**, pg. 723-733.

20. Barber, D.C., and Brown, B.H., [1985] "Recent developments in applied potential tomography--APT," in **Proc. 9th Int. Conf. Info. Proc. Med. Imaging**, Washington, D.C.

21. Santosa, F., and Vogelius, M., [1988] "A Backprojection Algorithm for Electrical Impedance Imaging," Institute for Physical Science & Technology, Univ. Maryland, Tech. Note BN-1081, July.

22. Huang, S.M., Plaskowski, A.B., Xie, G.C., and Beck, M.S., [1989] "Tomographic Imaging of Two-Component Flow using Capacitance Sensors," **J. Phys. E: Sci. Instrum., 22**, pg 173-177.

23. Beck, M., and Williams, R., [1990] "Looking into Process Plant," **The Chem. Engr., 26** July, pg. 14-15.

24. Kohn, R.V., and Vogelius, M., [1987] "Relaxation of a Variational Method for Impedance Computed Tomography," **Comm. Pure Appl. Math., 40**, pg. 745-777.

25. Kohn, R.V., and McKenney, A., [1989] "Numerical Implementation of a Variational Method for Electrical Impedance Tomography," Courant Institute of Mathematical Sciences, private communication.

26. Yorkey, T.J., [1986] **Comparing reconstruction methods for electrical impedance tomography**," Ph.D. Thesis, Dep. Elec. Comput. Eng., Univ. Wisc., Madison, WI 53706, August.

27. Yorkey, T.J., and Webster, J.G., [1987] "A comparison of impedance tomographic reconstruction algorithms," **Clin. Phys. Physiol. Meas., 8**, suppl. A, pg. 55-62.

28. Yorkey, T.J., Webster, J.B., and Tompkins, W.J., [1985] "Errors caused by contact impedance in impedance imaging," **Proc. Ann. Conf. IEEE Eng. Med. Biol. Soc., 7**, 1, pg. 632-637

29. Yorkey, T.J., Webster, J.G., and Tompkins, W.J., [1986] "An optimal impedance tomographic reconstruction algorithm," **Proc. Ann. Conf. IEEE Eng. Med. Biol. Soc., 8**, 1, pg. 339-342.

30. Yorkey, T.J., Webster, J.G., and Tompkins, W.J., [1987a] "An improved perturbation technique for electrical impedance imaging with some criticisms," **IEEE Trans. Biomed. Eng., 34**, 11, pg. 898-901.

31. Yorkey, T.J., Webster, J.G., and Tompkins, W.J., [1987b] "Comparing reconstruction algorithms for electrical impedance tomography," **IEEE Trans Biomed. Eng., 34**, PG. 843-852.

32. Brown, B.H., Barber, D.C., and Seagar, A.D., [1985] "Applied potential tomography - clinical applications," **IEEE Conf. Publ. (Inst. Electr. Eng.)**, No. 257, pg. 74-78.

33. Kim, Y., Webster, J.G., and Tompkins, W.J., [1983] "Electrical impedance imaging of the thorax," **J. Microwave Power, 18**, 3, pg. 245-257.

34. Fuks, L.F., Isaacson, D., Gisser, D.G., and Newell, J.C., [1989] "Tomographic Images of Dielectric Tissue Properties," **IEEE-Trans. Biomed. Eng.**, in review.

35. Cheng, K-S, Isaacson, D., Newell, J.C., and Gisser, D.G., [1989] "Electrode Models for Electric Current Computed Tomography," **IEEE-Trans. Biomed. Eng., 36**(9), pg. 918-924.

36. Cheney, M., Isaacson, D., Newell, J.C., Simske, S., and Goble, J., [1980] "NOSER: An algorithm for solving the inverse conductivity problem," **Int. J. Imaging. Systems and Tech., 2**, pg. 66-75.

37. Brown, B.H., and Barber, D.C., [1987] "Electrical impedance tomography; the construction and application to physiological measurement of electrical impedance images," **Medical Prog. Through Technology, 13**, pg. 69-75.

38. Brown, B.H., Karatzas, T., Nakielny, R., and Clarke, R.G., [1988] "Determination of upper arm muscle and fat areas using electrical impedance measurements," **Clin. Phys. Physiol. Meas. (UK), 9**, 1, pg. 47-55.

39. Gilbert, P., [1972] "Iterative methods for the reconstruction of three-dimensional objects from projections," **J. Theoret. Biol., 36**, pg. 105-117.

40. Griffiths, H., [1987] "The importance of phase measurement in electrical impedance tomography," **Phys. Med. Biol., 32**, 11, pg. 1435-1444.

41. Henderson, R.P., and Webster, J.G., [1978] "An impedance camera for spatially specific measurements of thorax," **IEEE Trans. Biomed. Eng., BME-25**, pg. 250-254.

42. Kagawa, Y., Murai, T., and Matsumoto, O., [1983] "Finite element iterative technique for determining the interface boundary between Laplace and Poisson domains--characteristic analysis of field effect transistor," **Int. J. Numer. Methods Eng., 19**, pg. 315-329.

43. Kardous, G., [1987] **Etude de la distribution de la sensibility d'un systeme circulaire multi-electrodes en vue de la reconstruction d'images d'impedance bio-electrique,** PhD Thesis, Institute National des Sciences Appliquees de Lyon, Villeirbanne, France.

44. Kim, Y., Tompkins, W.J., and Webster, J.G., [1982] "Medical body imaging using electrical impedance and nonlinear reconstruction," **Ann. Northwest Bioeng. Conf., 10**, pg. 298-303.

45. Carey, G.F., and Oden, J.T., [1984] **Finite Element Computational Aspects: Vol. 3**, Prentice-Hall, Englewood Cliffs, N.J.

46. Hestenes, M.R., and Stiefel, E., [1952] "Methods of Conjugate Gradients for Solving Linear Systems," **J. Res. NBS, 49**, 6, pg. 409-436.

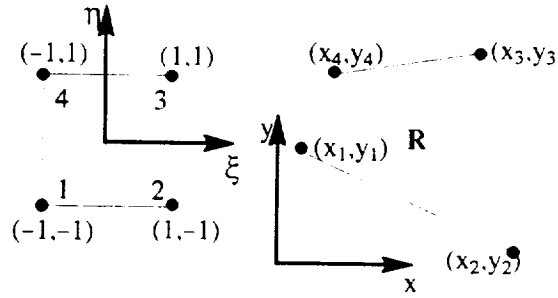

Figure 1. Quadrilateral element transformation geometry.

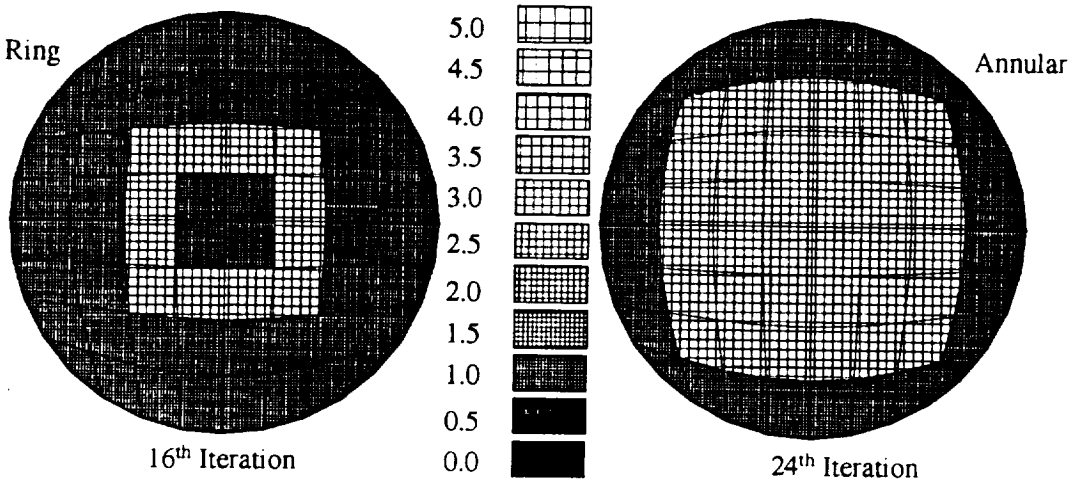

Figure 2. Converged patterns and resistivity index for both annular and ring geometries with zero permittivity. Contrast ratio: 3:1.

Third International Conference on Inverse Design Concepts and Optimization in Engineering Sciences (ICIDES-III), Editor: G.S. Dulikravich, Washington, D.C. October 23-25, 1991

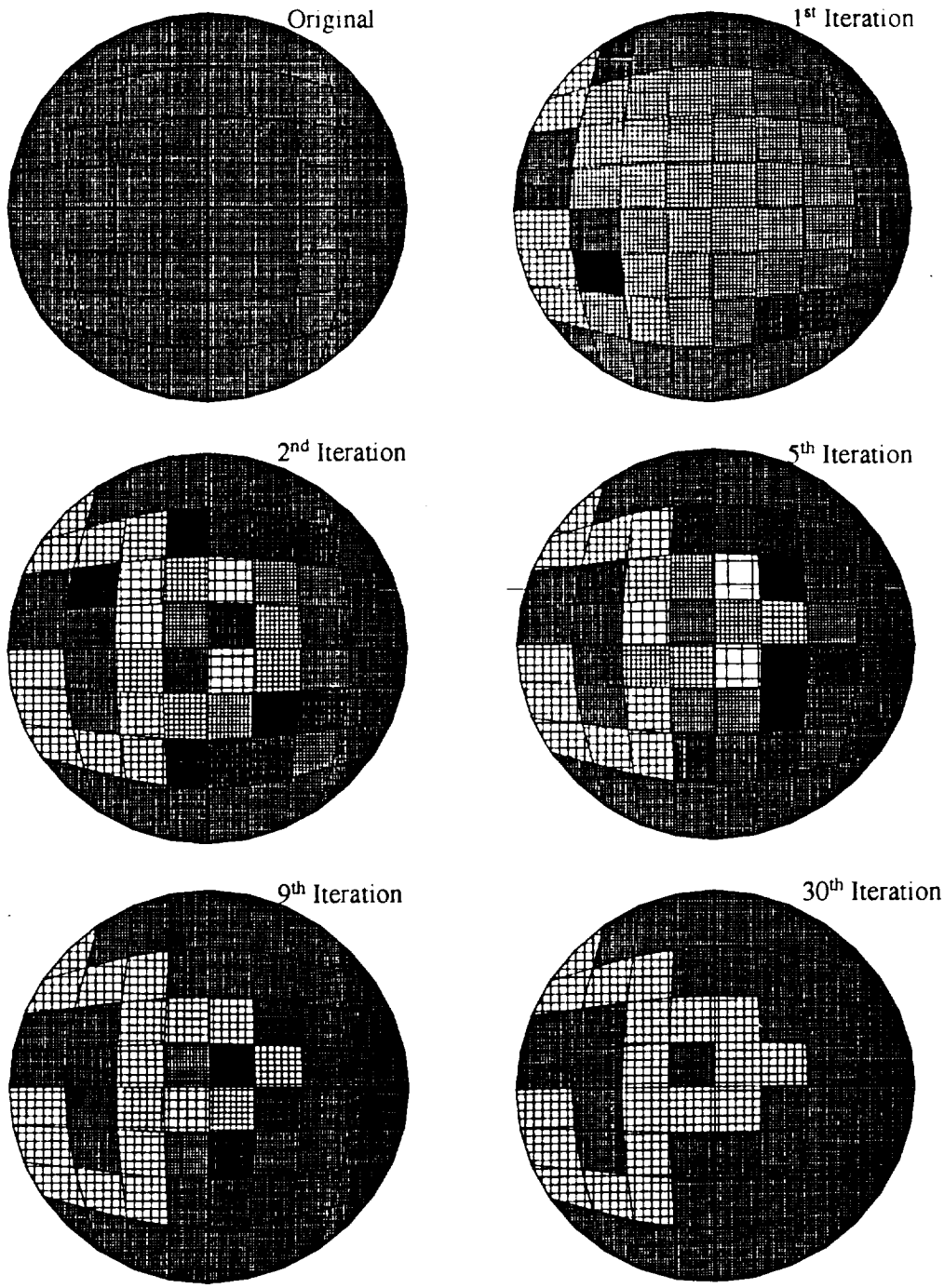

Figure 3. Typical convergence sequence for a 64 element array of quadrilateral elements with zero permittivity. Contrast ratio: 3:1.

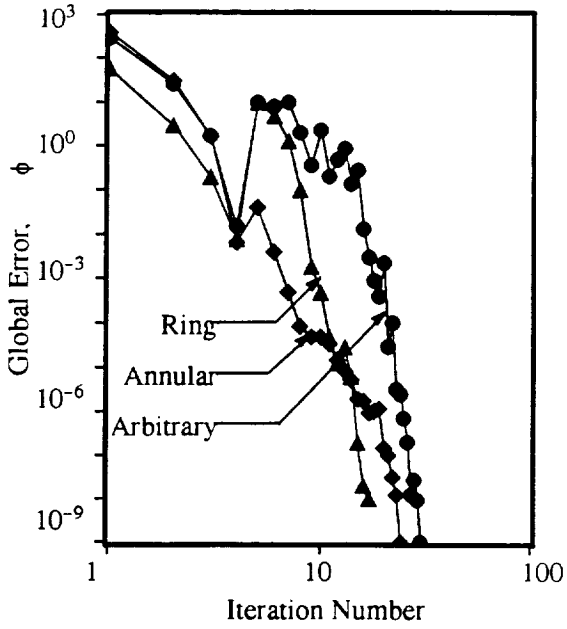

Figure 4. Global error for the three patterns tested.

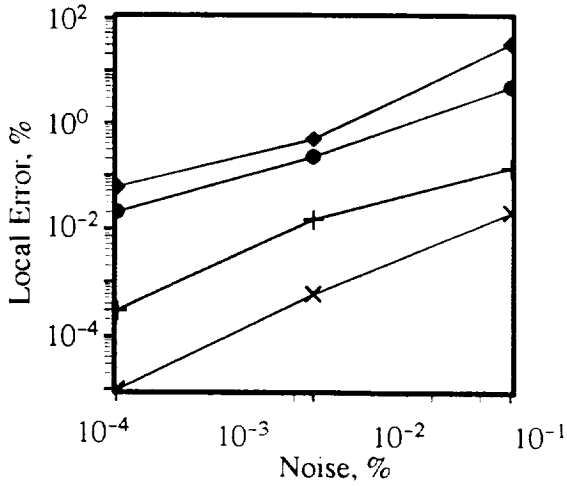

Figure 6. Local error for the annular-flow-like geometry. ♦ Inner Cells; • Inner Middle; + Outer Middle; x Outer Cells.

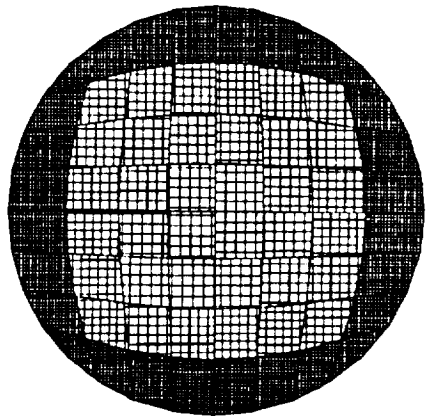

Figure 7. Converged annular pattern with 1% Gaussian noise.

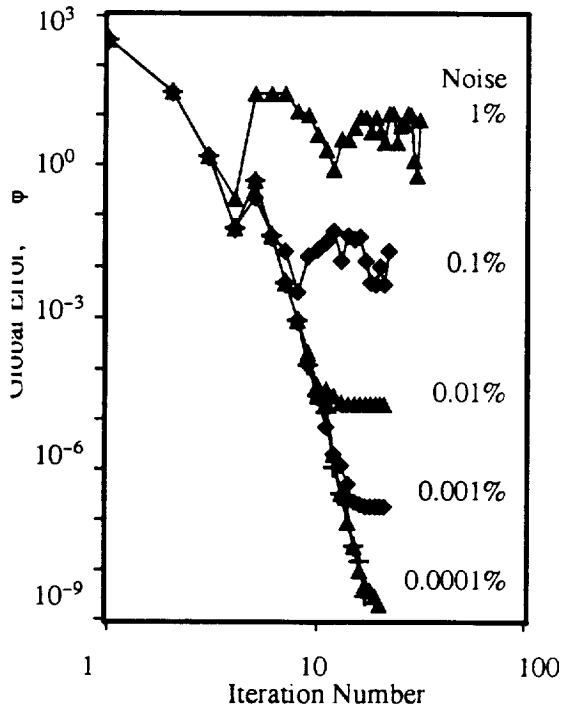

Figure 5. Effect of noise on convergence for the annular pattern.

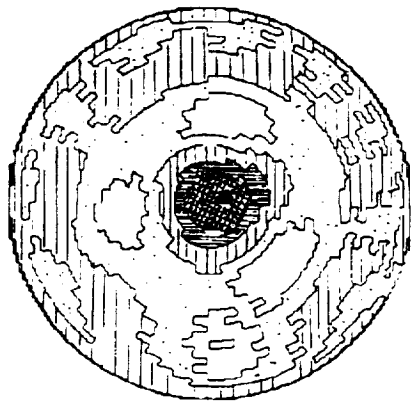

Figure 8. Example of electrical impedance reconstruction of an air-water system using the NOSER method.[36]